OXFORD UNIVERSITY PRESS | Human Molecular Genetics

Primary angle closure glaucoma (PACG) susceptibility gene PLEKHA7 encodes a novel Rac1/Cdc42 GAP that modulates cell migration and blood-aqueous barrier function

Journal:	*Human Molecular Genetics*
Manuscript ID	HMG-2017-TWB-00214.R2
Manuscript Type:	1 General Article - US Office
Date Submitted by the Author:	17-Jul-2017
Complete List of Authors:	Lee, Mei Chin; Singapore Eye Research Institute, Ocular Genetics; Singapore National Eye Centre, Glaucoma; Duke-NUS Medical School, The Ophthalmology & Visual Sciences Academic Clinical Program Shei, William; Singapore Eye Research Institute, Ocular Genetics Chan, Anita; Singapore National Eye Centre, Glaucoma; Duke-NUS Medical School, The Ophthalmology & Visual Sciences Academic Clinical Program Chua, Boon Tin; Institute of Molecular and Cell Biology, IMCB-NCC MPI Singapore Oncogenome Programme Goh, Shuang Ru; Singapore Eye Research Institute, Ocular Genetics Chong, Yaan Fun; Singapore Eye Research Institute, Singapore Eye Research Institute Hilmy, Maryam; Singapore General Hospital, Patholgy Nongpiur, Monisha; Singapore Eye Research Institute, Glaucoma; Singapore National Eye Centre, Glaucoma; Duke-NUS Medical School, The Ophthalmology & Visual Sciences Academic Clinical Program Baskaran, Mani; Singapore Eye Research Institute, Glaucoma; Singapore National Eye Centre, Glaucoma; Duke-NUS Medical School, The Ophthalmology & Visual Sciences Academic Clinical Program Khor, Chiea; Genome Institute of Singapore, Infectious Diseases; Singapore Eye Research Institute, Ocular Genetics; National University of Singapore, Biochemistry Aung, Tin; Singapore Eye Research Institute, Ocular Genetics; Singapore National Eye Centre, Glaucoma; Duke-NUS Medical School, The Ophthalmology & Visual Sciences Academic Clinical Program; National University of Singapore, Ophthalmology Hunziker, Walter; Institute of Molecular and Cell Biology, Epithelial Cell Biology; Singapore Eye Research Institute, Ocular Genetics; National University of Singapore, Physiology VITHANA, ERANGA; Singapore Eye Research Institute, Singapore Eye Research Institute; Duke-NUS Medical School, The Ophthalmology & Visual Sciences Academic Clinical Program
Key Words:	PLEKHA7, Rac1, Cdc42, PACG, Blood Aqueous Barrier

Primary angle closure glaucoma (PACG) susceptibility gene PLEKHA7 encodes a novel Rac1/Cdc42 GAP that modulates cell migration and blood-aqueous barrier function

Mei-Chin Lee[1,2], William Shei [1], Anita S Chan[2,3], Boon-Tin Chua[8], Shuang-Ru Goh[2], Yaan-Fun Chong [2], Maryam H Hilmy [4], Monisha E Nongpiur [1,2], Mani Baskaran [1,2,3], Chiea-Chuen Khor [1,5,6], Tin Aung [1,2,3,7], Walter Hunziker [1,8,9*], and Eranga N Vithana [1,2*]

[1]Ocular Genetics Research Group; Singapore Eye Research Institute;

[2]The Ophthalmology & Visual Sciences Academic Clinical Program; Duke-NUS Medical School;

[3] Department of Glaucoma; Singapore National Eye Centre;

[4] Department of Pathology; Singapore General Hospital;

[5] Department of Human Genetics; Genome institute of Singapore; Agency for Science Technology and Research;

[6] Department of Biochemistry; National University of Singapore;

[7]Department of Ophthalmology; National University of Singapore;

[8]Institute of Molecular and Cell Biology; Agency for Science Technology and Research;

[9]Department of Physiology; National University of Singapore.

*Co-correspondence

Corresponding author:

A/Prof Eranga Vithana

The Academia, 20 College Road, Discovery Tower level 6, Singapore 169856

Phone: (65)6576 7216 Fax: (65)62252568

E-mail: eranga.n.v@sericom.sg

Abstract

PLEKHA7, a gene recently associated with primary angle closure glaucoma (PACG), encodes an apical junctional protein expressed in components of the blood aqueous barrier (BAB). We found that *PLEKHA7* is down-regulated in lens epithelial cells and in iris tissue of PACG patients. *PLEKHA7* expression also correlated with the C risk allele of the sentinel SNP rs11024102 with the risk allele carrier groups having significantly reduced *PLEKHA7* levels compared to non-risk allele carriers. Silencing of *PLEKHA7* in human immortalized non-pigmented ciliary epithelium (h-iNPCE) and primary trabecular meshwork cells, which are intimately linked to BAB and aqueous humor outflow respectively, affected actin cytoskeleton organization. PLEKHA7 specifically interacts with GTP-bound Rac1 and Cdc42, but not RhoA, and the activation status of the two small GTPases is linked to PLEKHA7 expression levels. PLEKHA7 stimulates Rac1 and Cdc42 GTP hydrolysis, without affecting nucleotide exchange, identifying PLEKHA7 as a novel Rac1/Cdc42 GAP. Consistent with the regulatory role of Rac1 and Cdc42 in maintaining the tight junction permeability, silencing of PLEKHA7 compromises the paracellular barrier between h-iNPCE cells. Thus, downregulation of PLEKHA7 in PACG may affect BAB integrity and aqueous humor outflow via its Rac1/Cdc42 GAP activity, thereby contributing to disease etiology.

Introduction

Glaucoma is the leading cause of irreversible blindness worldwide. Categorized according to the anatomy of the anterior chamber angle, there are two main forms of glaucoma, primary open angle glaucoma (POAG) and primary angle closure glaucoma (PACG). PACG is a major form of glaucoma in Asians, with 77% of the estimated 15.5 million people afflicted with PACG living in Asia (1-3). PACG results from obstruction of the trabecular meshwork by the iris to the outflow of aqueous, leading to raised intraocular pressure (IOP) and irreversible damage to the optic nerve. Evidence suggests that the pathogenesis of PACG is complex with multiple contributing factors including biometric/anatomical, physiological and genetic factors. Genome wide association studies in large patient cohorts of PACG have uncovered eight distinct genetic loci that are beginning to shed light into possible mechanisms involved in PACG(4, 5). The *PLEKHA7* susceptibility locus on chromosome 11 showed one of the strongest statistical evidences of PACG association on an expanded GWAS, and credible set analysis conclusively bounded the association to *PLEKHA7* instead of the nearby genes (4). Thus, we prioritized this gene for further molecular characterization. *PLEKHA7* encodes a protein that localizes to the apical junctional complex (AJC) within components of the blood aqueous barrier (BAB) and also to mechanosensitive components in the eye; suggesting that a compromised BAB and abnormal dynamic mechanosensory mechanisms in ocular structures may contribute to the pathogenesis of PACG (6-8). Indeed, silencing the expression of constituents of tight junctions (TJs), a structure of the AJC, of Schlemm's canal endothelia, has recently been shown to enhance humor outflow in the mouse eye (9).

Principal sites of the BAB include the tight junctions of the non-pigmented ciliary epithelium (NPCE), the iris capillary endothelial cells and the posterior iris epithelium (10). Together, they restrict or regulate the movement of macromolecules, such as plasma proteins, or solutes from the capillaries of ciliary body and the iris into the anterior chamber (10, 11). Prior studies implicated a breakdown of the BAB and leakage of inflammatory proteins as a mechanism contributing to the IOP rise seen in PACG (7, 12, 13). Expression of PLEKHA7 in cells linked to the formation of the BAB further supported a potential connection between PLEKHA7, BAB deregulation and PACG.

PLEKHA7 was initially identified as a microtubule adaptor that exist in a complex with Nezha and KIFC3 (14). In addition, PLEKHA7 has been linked to actin based adhesion complexes through interactions with afadin (15) and the recruitment of paracingulin and PDXD11 to epithelial AJs (16, 17). However a clear cellular or molecular mechanism of how PLEKHA7 may be involved in the maintenance of BAB is not known.

Paracellular barrier function in different epithelial and endothelial cell types requires AJCs (18, 19) and is regulated by Rho GTPases (20-26). For example, the activity of the Rho GTPases Rac1 and RhoA can be regulated by AJC protein paracingulin through the recruitment of Tiam1 and GEF-H1(27). Since PLEKHA7 directly interacts with paracingulin (15, 16), it is conceivable that it also regulates the BAB. Alterations in PLEKHA7, as they occur in PACG, could therefore result in the barrier changes observed in these eyes by altering the optimal functioning of the AJCs and contribute to the etiology of PACG.

In this study we aimed to characterize molecular mechanism(s) of *PLEKHA7* in ocular cells in order to understand how PLEKHA7 contributes to the etiology of PACG. Our investigation uncovered low *PLEKHA7* expression levels in lens epithelial cells of PACG patients. Hence, we analyzed the effect of silencing PLEKHA7 in primary human trabecular meshwork (HTM) and human immortalized non-pigmented ciliary epithelium (h-iNPCE) cells, key components of aqueous humor outflow pathway and BAB respectively that are also important in glaucoma. We found that modulation of PLEKHA7 protein level in conventional 2-dimensional (2-D) culture lead to changes in the actin cytoskeleton structure, migration and the barrier permeability likely via Rac1 and Cdc42 signalling pathways. Above all, we have revealed PLEKHA7 as a direct interacting GAP for both Rac1 and Cdc42 that can stimulate GTP hydrolysing activity critical for cellular barrier integrity. The effects of altered PLEKHA7 expression level on barrier integrity were also evaluated in 3-dimensional (3-D) spheroidal cultures of h-iNPCE cells. Our data highlight that PLEKHA7 expression level affect cellular barrier integrity, suggesting that barrier defects due to reduced PLEKHA7 level contributes to the etiology of PACG.

Results

Differential expression of PLEKHA7 in PACG patients

The minor C allele of the intragenic SNP rs11024102, located in intron 3 of *PLEKHA7,* was consistently associated with increased risk of PACG (4, 5). To investigate its role in PACG pathogenesis, we compared *PLEKHA7* expression levels between control (non-glaucoma), PACG and primary open angle glaucoma (POAG) subjects. Lens capsules, which are more readily available, were obtained from 53 control, 39 PACG and 64 POAG subjects and relative *PLEKHA7* mRNA expression was analyzed by real-time qPCR. Values from non-glaucoma subjects were applied as baseline for the calculation of fold changes in *PLEKHA7* gene expression (Fig. 1A). The analysis revealed that *PLEKHA7* gene expression was significantly lower in PACG lens capsules as compared to the non-glaucoma control lens capsules ($p=1.03\times10^{-9}$) (Fig. 1A). in contrast to PACG, *PLEKHA7* was significantly upregulated in POAG subjects (p=0.0003) when compared to expression in control lens capsules (Fig. 1A). We also analysed iris tissues of 20 PACG and 20 POAG subjects for mRNA expression of *PLEKHA7*. Since there was no availability of non-glaucoma iris tissues, we used the data from the POAG subjects as baseline values for comparisons of fold changes in gene expression of PACG subjects. Between the two glaucoma subtypes, PACG expressed significantly lower fold expression of *PLEKHA7* (0.80±0.15, p=0.0015) (Fig. 1B).

Next, we assessed whether the genotypes of the *PLEKHA7* rs11024102 T>C sentinel marker correlated with PLEKHA7 expression levels in the lens capsule, the only tissues for which there was corresponding genomic DNA available from patients. We therefore stratified our PACG samples (N=26) by their genotypes (risk C/C, non-risk T/T, and heterozygous C/T) with respect to rs11024102 and analyzed PLEKHA7 expression level. The expression level of *PLEKHA7* was found to correlate significantly with the presence of the risk allele. In PACG lens capsules, *PLEKHA7* mRNA expression was significantly down regulated in C/T heterozygotes (0.67±0.07, (p=0.034) and in C/C homozygous risk allele carriers (0.76±0.05, p=0.025) when compared with individuals homozygous for the T/T wild-type allele (Fig. 1C).

As a comparison, we also assessed whether the *PLEKHA7* rs11024102 T>C genotype correlated with *PLEKHA7* expression levels in the POAG lens capsule samples (N=52) and normal subjects (N=24). Among the POAG lens capsule samples, 34.61% were homozygous for the non-risk allele, 57.69% were heterozygous and 7.69% were homozygous for the risk allele of rs11024102. In POAG subjects *PLEKHA7* mRNA expression was significantly (p=0.001) upregulated in C/T heterozygotes, but expression was not significantly different in C/C homozygous risk allele carriers when compared with individuals homozygous for the T/T wild-type allele (Fig. 1D). In the control group, *PLEKHA7* mRNA expression was not significantly different between the C/T heterozygotes and T/T homozygotes (Fig. 1E).

Analysis of genomic region near SNP rs11024102

The index rs11024102 SNP was found to be located close to multiple regulatory functional elements using data from the publicly available ENCODE and HaploReg (28) databases (Supplementary Material, Fig. 1 and Table S1). Due to the substantial distance between rs11024102 and exon-intron boundaries, we speculate that rs11024102 may exert a quantitative, regulatory effect of gene expression rather than splicing or other qualitative changes. To this end, we looked up publicly available databases where expression quantitative trait (eQTL) data is accessible (GTEx(29) and HaploReg(28)). The data suggest that rs11024102 and SNP in LD with it (defined as pairwise r2>0.8) could serve as eQTLs for the neighbouring OR7E14P in lung and skin tissue (HaploReg $P < 1 \times 10^{-6}$). A further search of a whole blood eQTL(30) database yielded suggestive evidence for rs11024102 to be an eQTL for *PLEKHA7* (GRASP P = 0.00018). However, none of these publicly available databases were informative for eye tissues, which would be most relevant for our study on PACG and POAG. We also analyzed DNAse1 hypersensitivity sites (depicting potential sites where the chromatin is open and thus accessible for transcription factor binding) at the *PLEKHA7* locus, centered upon the sentinel SNP rs11024102. DNAse1 sensitive sites were indicated for several cell lines, but none were detected for eye related tissue such as the retinal epithelial cell line

(Supplementary Material, Fig. 1a). More functional investigations would be needed to elucidate the role of rs11024102 as harbouring a site sensitive to the regulation of *PLEKHA7* via binding of transcription factors to open chromatin.

PLEKHA7 is important for organization of the cytoskeleton

To mimic the reduced PLEKHA7 mRNA expression observed in PACG subjects, primary HTM cells were transfected with a PLEKHA7-specific shRNA construct (pLKO-MS3), resulting in depletion of PLEKHA7 protein (Fig. 2A). Fluorescence microscopy of HTM cells stained with a specific antibody to PLEKHA7 (Supplementary material, Fig. S2) and actin revealed extensive colocalization in control cells (Fig. 2B and D). Depletion of PLEKHA7 resulted in loss of actin cytoskeletal structures and rounding of HTM cells (Fig. 2C and D). By 24h post-transfection, actin had redistributed to a perinuclear patch that co-localized with the residual PLEKHA7 (Fig. 2C). Thus, PLEKHA7 co-localizes with filamentous actin and is critical in maintaining cytoskeletal organization.

PLEKHA7 associates with Rac1 and Cdc42 and stimulates their GTPase activity

Given the important role of Rho GTPases in regulation of actin dynamics, we next explored if PLEKHA7 co-localized with Rac1, Cdc42 or RhoA. Since some of these GTPases show distinct subcellular distributions in migrating cells (31-33), we wounded h-iNPCE cell monolayers and stained cells with antibodies to PLEKHA7 or the GTP-bound forms of Rac1, Cdc42 and RhoA (Fig. 3A). Rac1-GTP, as expected, was enriched at the cell periphery in the leading edge of migrating cells, where it extensively co-localized with PLEKHA7 (Fig. 3A top panel and B). PLEKHA7 also co-localized with Cdc42-GTP to a perinulcear structure reminiscent of the Golgi complex (Fig. 3A middle panel and B), which during collective cell migration polarizes towards the leading edge of the cells (34). In contrast to the extensive co-localization with Rac-1-GTP and Cdc42-GTP, PLEKHA7 showed little co-localization with RhoA-GTP (Fig. 3A bottom panel and B).

To test if PLEKHA7 is in a complex with Rac1 or Cdc42, we co-immunoprecipitated endogenous PLEKHA7 and probed for the presence of the respective Rho GTPases in the precipitated complex. Both Rac1 and Cdc42, but not RhoA, coprecipitated with PLEKHA7 (Fig. 3C). Thus, in

agreement with the co-localization data (Fig. 3 A and B), PLEKHA7 can associate with complexes containing Rac1 and Cdc42.

To determine if PLEKHA7 binds Rac1 or Cdc42 directly and whether there is a preferential association with either the GTP or GDP bound forms of the GTPases, purified recombinant GST-PLEKHA7 together with GDP or GTPγS loaded His-Rac1 or His-Cdc42 were used for *in-vitro* binding assays. Results revealed that PLEKHA7 can directly interact with Cdc42 and Rac1 and preferentially binds the GTP-bound form of the two small GTPases as compared to the empty or GDP-bound forms (Fig. 3D and E).

Given the lower PLEKHA7 expression levels in PACG subjects (Fig. 1), we next analyzed if silencing of PLEKHA7 affects Cdc42 and Rac1 activation levels. To probe the activation state of Cdc42 or Rac1 we took advantage of the specific interaction of the protein binding domain of the p21 activated kinase 1 effector with the GTP but not the GDP bound forms of Rac1 and Cdc42 (35). Silencing of PLEKHA7 in h-iNPCE cells resulted in a 50% decrease in Cdc42-GTP and Rac1-GTP protein, while overexpression increased the amount of activated Cdc42 and Rac1 by 80% (Fig. 4A-C).

Many guanine nucleotide-exchange factors (GEF) and GTPase-activating proteins (GAP) for RhoGTPases have a conserved PH domain. Since a PH domain is also present in PLEKHA7, we tested if PLEKHA7 could act as a potential GEF or GAP for Cdc42 or Rac1 in in vitro assays. To assess GAP activity, the effect of purified full length GST-PLEKHA7 on the rate of GTP hydrolysis was determined by CytoPhos reagent that detects the inorganic phosphate released from hydrolysis of GTP bound to the respective RhoGTPase. PLEKHA7 GAP activity toward Cdc42 and Rac1 was significantly stimulated over the intrinsic GTPase activity of either recombinant His-tagged Cdc42 (Fig. 4D) or Rac1 (Fig. 4E). In contrast, no significant nucleotide exchange activity beyond its intrinsic GEF activity of PLEKHA7 on GDP loaded Cdc42 or Rac1 (Fig. 4F and G) was observed, indicating that PLEKHA7 acts as a GAP for Cdc42 and Rac1.

PLEKHA7 modulates cell migration

Rac1 and Cdc42 play important roles in cell migration, where they regulate actin dynamics in lamellipodia and filopodia at the leading edge of the migrating cell (36, 37). To evaluate if PLEKHA7, presumably through its action on the small GTP binding proteins, regulates this process, we performed scratch wound closure assays with h-iNPCE cells where PLEKHA7 was either overexpressed or silenced. As monitored by time-lapse imaging, a significantly faster (60%) wound closure was observed for cells overexpressing PLEKHA7 (Fig. 5A and B). In contrast, cells with reduced PLEKHA7 protein levels closed the wound slower (30%) compared to controls, and this was rescued by transfection of a PLEKHA7 cDNA. As expected, Rac-GTP was enriched in lamellipodia at the leading edge of migrating cells, where it showed extensive colocalization with PLEKHA7 (Fig. 5C). Structured illumination microscopy (3D-SIM) (38), to analyze the colocalization at nanoscale resolution, confrimed the extensive colocalization of Rac1-GTP and PLEKHA7 to small punctate structures enriched at the leading edge of cells (Fig. 5D).

***PLEKHA7 modulates paracellular* barrier permeability**

Besides cell migration, Rac1 and Cdc42 are well established modulators of the paracellular barrier (21, 39-41). Furthermore, PLEKHA7 interacts with paracingulin (16), which has been detected at both AJs and TJs (42) and recruits GEFs for Rac1 and RhoA (27). To test a possible role of PLEKHA7 in barrier function, we used both 2-D monolayer and 3-D spheroid culture models (43) of h-iNPCE cells where PLEKHA7 was either overexpressed or silenced.

Since an intact barrier requires the recruitment of junctional proteins to the AJC (44-49), we first analyzed the localization of PLEKHA7, occludin (a TJ marker protein) and β-catenin (an AJ marker protein) in spheroids of PLEKHA7 overexpressing or depleted h-iNPCE cells. Both occludin and β-catenin localized to sites of cell-cell contact in the control spheroids and this was not affected by overexpressing PLEKHA7 (Fig. 6A). Confocal imaging of z-stacks confirmed colocalization of PLEKHA7 and occludin at the apical pole of the outermost cell layer of h-iNPCE spheroids (Supplementary Material, Fig. S3). In contrast, overall and junctional staining for these proteins was strongly reduced in PLEKHA7 depleted spheroids. Interestingly, western blot analysis showed higher

or lower levels of occludin and β-catenin in spheroids where PLEKHA7 had been overexpressed or silenced, respectively (Fig. 6C), suggesting that the presence of PLEKHA7 could stabilize these proteins at cellular junctions.

Next, we assessed barrier permeability in live spheroids from h-iNPCE cells where PLEKHA7 had been overexpressed or silenced, by monitoring accessibility of a 4kDa fluorescein isothiocyanate (FITC) labelled dextran as an indicator to determine paracelllular permeability changes of TJ (50).Consistent with a compromised barrier, strong labeling by dextran FITC was observed in spheroids from cells where PLEKHA7 had been depleted, while spheroids from control cells or cells overexpressing PLEKHA7 showed background labeling consistent with exclusion of the tracer. Re-expression of PLEKHA7 rescued the barrier defect in spheroids from cells where PLEKHA7 had been silenced (Fig. 6D).

The effect of PLEKHA7 on barrier function was further corroborated on 2-D h-iNPCE cell monolayers using real time impedance measurements. PLEKHA7 overexpression enhanced barrier function as assessed by higher cumulative impedance across cell monolayers, while silencing of PLEKHA7 with vector-based shRNA construct pLKO-MS3 (Fig. 6E and F) or pLKO-MS2 (Supplementary Material, Fig. S4) compromised the barrier as compared to control cells. To test if PLEKHA7 expression levels would affect the kinetics in assembly of functional adherens junction complexes (composed of both AJ and TJ) we applied calcium switch assays. Interestingly, depletion of Ca^{2+} by EDTA induced a milder perturbance of the barrier on PLEKHA7 overexpressing cells as compared to controls, whereas the barrier in cells where PLEKHA7 was depleted became more sensitive to EDTA. Furthermore, the kinetics of barrier recovery in PLEKHA7 overexpressing cells after EDTA washout and was faster, whereas depleted of PLEKHA7 showed a delayed recovery (Fig. 6G).

PLEKHA7 and Rac1 co-localize in tissues of the BAB in the eye

Above we showed that PLEKHA7 co-localizes with Rac1-GTP and Cdc42-GTP in h-iNPCE cells. To confirm that these proteins also co-localize in the eye, and in particular in structures

implicated in PACG and associated with the BAB, we stained ocular sections for PLEKHA7 and Rac1-GTP or Cdc42-GTP. In agreement with the cell culture data, extensive co-localization of PLEKHA7 with Cdc42-GTP was observed in ciliary muscle (CM), NPCE (Fig. 7A), trabecular meshwork (TM), iris dilator muscle (IDM) and iris capillaries (IC). PLEKHA7 also co-localized in similar structures when co-stained with Rac1-GTP (Fig. 7B).

Discussion

This study was undertaken to better understand the molecular and cellular mechanisms of the PACG associated gene, *PLEKHA7*. By examining PACG clinical samples such as lens capsules and iris tissues, this study provides important insights into the role of PLEKHA7 in the eye. In the lens capsules, we show that *PLEKHA7* mRNA expression is significantly reduced in PACG subjects compared to controls. *PLEKHA7* expression in iridial tissues is also significantly reduced in PACG subjects compared to POAG subjects.

However, the analysis of genotypic expression of *PLEKHA7* in PACG, POAG and normal lens capsules indicated that *PLEKHA7* expression is rather more complex. In PACG, the expression level of *PLEKHA7* correlates to the C risk allele of the sentinel SNP rs11024102 of PLEKHA7, as the risk allele carrier groups have significantly reduced *PLEKHA7* levels compared to non-risk allele carriers. Although there is more marked reduction of *PLEKHA7* in the PACG heterozygous group than in the homozygous risk group (Fig. 1C) this may be attributed to the small sample size of the latter group. We did not observe any genotypic specific expression differences among a similar number of normal lens capsule samples. Among the POAG cases, the heterozygotes, which was the largest group within this cohort, had a significantly higher *PLEKHA7* expression than the non-risk allele carriers, reflecting the prior observation that *PLEKHA7* is upregulated in POAG compared to the controls (Figure 1A). These differences in allele specific expression may be due to differences in epigenetic phenomena between the two case groups (involving the genomic region that includes rs11024102) or a trans effect involving differences in expression of another molecule interacting with the genomic region that includes rs11024102. It is also possible that secondary factors such IOP and

IOP reducing medications have affected the expression in one case group more than the other. Regardless of the underlying mechanisms at play at the genetic locus to affect expression, our data indicate that *PLEKHA7* is downregulated in the analysed anterior segment tissues of PACG patients compared to both POAG and normal controls.

Although *PLEKHA7* rs11024102 is a very robustly associated marker for PACG, our deep resequencing effort on the *PLEKHA7* locus did not identify a causative variant (e.g. splice variant, amino acid substitution, or stop codon) responsible for the strong association between the PACG disease and SNP rs11024102. Thus, rs11024102 remains the strongest associated *PLEKHA7* variant to date. According to eQTL data in HaploReg(28), rs11024102 and SNPs in LD with it (defined as pairwise r2>0.8) could serve as eQTLs for the neighbouring OR7E14P (HaploReg P < 1 x 10-6) and there is tentative suggestion for rs11024102 to be an eQTL for *PLEKHA7* (GRASP P = 0.00018). However, data from the latest release of the GTEx browser (https://www.gtexportal.org/home/) indicate that the rs11024102 SNP does not act as a significant eQTL for any gene across all tissues analyzed in the GTEx portal. Moreover, none of these publicly available databases were informative for eye tissues, which would be most relevant for our study on PACG and POAG. Testing for the effects of rs11024102 on gene expression, using pGL3 luciferase reporter assays in relevant cell lines, as done in the case of *EPO* gene and alleles of rs1617640 (51), is also made difficult by the fact that rs11024102 is located deep within intron 3 of *PLEKHA7* (Supplementary Material, Fig. S1) and not upstream of transcription start site of *PLEKHA7*. We suggest that further experimentation await the discovery of other non-coding variants more likely to be causal at this PACG locus and also better candidates for impacting *PLEKHA7* expression.

Nevertheless, reduced levels of PLEKHA7 in two separate anterior segment tissues in PACG suggest causality, albeit indirect, in the absence of the causal mutation. The down-regulation of *PLEKHA7* observed in PACG subjects thus corroborates our GWAS finding implicating aberration of PLEKHA7 as a contributing factor to PACG disease. Together with our previous finding that PLEKHA7 colocalizes with apical junctional complexes of cells of the BAB, this low PLEKHA7 expression levels in lens capsule and iris tissues, the latter that may regarded as a PACG affected

tissue suggests that the BAB may be a contributing causative factor in PACG. To support this, we modulated PLEKHA7 levels and demonstrated a barrier defect by the ability for FITC-dextran to penetrate h-iNPCE spheroids with reduced PLEKHA7 protein. Biochemical assays and fluorescent staining also showed that the PLEKHA7 interacts and regulates Rac1 and Cdc42, molecules well known to affect tissue barrier permeability.

As members of the Rho family of small GTPases (Rac1, Cdc42 and RhoA) are intimately linked to the regulation of actin cytoskeleton (52, 53) and PLEKHA7 has been indirectly linked to regulating RhoA and Rac1 activity via cingulin and paracingulin (27, 42), PLEKHA7 association with Rho family GTPAses was further explored using h-iNPCE cells induced to migrate in a wound closure assay. We found that PLEKHA7 extensively colocalized with Rac1 and Cdc42 in lamellipodia and in a perinulcear compartment, respectively, but less so with RhoA. Binding experiments using purified PLEKHA7 and the Rho family GTPases confirmed a direct interaction of PLEKHA7 with Rac1 and Cdc42, but not RhoA, in agreement with the colocalization experiments. Rho GTPases undergo a cycle whereby an exchange factor or GEF catalyses the exchange of GDP for GTP to activate the small GTP binding protein, allowing it to bind to downstream effectors. Here, our findings indicated Rac1 and Cdc42 are direct interactors of PLEKHA7 and the latter functioned as GTPase GAP mechanistically. These interactions affect the downstream effector molecules of the Rac1and Cdc42 GTPases in a PLEKHA7 expression-dependent manner. Thus, lowered PLEKHA7 in PACG could affect barrier permeability. PLEKHA7 was revealed to be a GAP that was found to preferentially bind to activated forms of Rac1 and Cdc42 (e.g. Rac1-GTP and Cdc42-GTP) thereby stimulating their intrinsic GTPase activities. Interestingly, since paracingulin also recruits the Rac1 GEF Tiam1, and since PLEKHA7 is essential for recruiting paracingulin to the TJ (16, 27), it is possible that paracingulin may in fact function as a scaffold to recruit both GAP (PLEKHA7) and a GEF (Tiam1) in a spatially restricted fashion and collectively stage PLEKHA7 as a molecule that could orchestrate Rho GTPases pathway.

In wound-closure assays, PLEKHA7 showed a striking colocalization with differentially distributed Rac1 and Cdc42 in migrating h-iNPCE cells. Lamellipodia, which are regulated by Rac1,

extend at the leading edge of migrating cells (54) and the Golgi complex reorients in the direction of cell migration (34). PLEKHA7 colocalized with Rac1 to punctate structures, possible focal adhesions, enriched in the leading edge. In addition, PLEKHA7 was present with Cdc42 in a perinuclear compartment, likely the Golgi complex. A localization of Cdc42 to the Golgi complex is well established (55), where it has been implicated in both actin and microtubule dependent functions, including cell migration and Golgi positioning (56). Thus, the effects that modulating PLEKHA7 expression had on cell migration could reflect PLEKHA7 involvement as a GAP in rapid reorganization of cytoskeletal structure involving Rac1, Cdc42 or both.

Spatial regulation of actin dynamics at the AJC is critical for establishment and maintenance of cell polarity (36, 37) and both Rac1 and Cdc42 are important for barrier function (40, 57). The localization of PLEKHA7 to the AJC is well established (6, 16). Rapid reorganization of cytoskeletal structures and signal transduction are often dependent on the type of stimulus and the differential regulation of Rho GTPases (52, 53). In our experiments, depletion of PLEKHA7 in 2D h-iNPCE cell monolayers reduced the barrier integrity, while in the calcium switch assays, overexpression of PLEKHA7 significantly enhanced barrier re-establishment.

Similar data was obtained in a 3D-spheroid permeability assay using FITC-dextran with polarized h-iNPCE, providing an alternative model for assessment of PLEKHA7 role in regulating paracellular permeability. Indeed, silencing of PLEKHA7 compromised paracellular barrier integrity and this effect can be rescued by overexpression of PLEKHA7. While depletion of PLEKHA7 in MDCK cells did not to affect recruitment of E-cadherin, β-catenin and ZO-1 (16), over-expression of PLEKHA7 in h-iNPCE cells affected recruitment of both TJ occludin and also AJ β-catenin, which could explain the effects of modulating PLEKHA7 levels on the paracellular barrier in tissue-specific context.

PLEKHA7 expression is reduced in PACG patients. Silencing of PLEKHA7 in h-iNPCE cells and primary HTM cells which are the ocular cells involved in PACG, affects actin cytoskeletal structure, cell migration, adhesion and paracellular barrier function (Fig. 8). These effects are likely

mediated through the GAP activity of PLEKHA7 on Rac1/Cdc42, which are well-established regulators of cell-cell adhesion and paracellular barrier function (58-60). PLEKHA7 and Rac1/Cdc42 colocalized in situ, at principal BAB sites such as the NPCE and iris vasculature as well as the trabecular meshwork, a major component of the ocular aqueous humor outflow pathway. Extrapolation of our experimental findings to PACG patients, suggests that the reduction in PLEKHA7 expression may result in a "leaky" BAB due to less recruitment of TJ or AJ proteins in the paracellular regions of NPCE and iris vascular endothelial cells, where PLEKHA7 was explicitly localised to in our previous immunohistochemistry studies in human eyes (6). This "leaky" BAB may therefore contribute to PACG by allowing unwanted entry of undesired serum proteins into the anterior chamber (61, 62), which then cause a sub clinical inflammatory response, increasing the risk of peripheral anterior synechiae formation in both acute and chronic angle closure glaucoma.

During dilation, a dynamic increase in iris volume or its lesser reduction is also seen in eyes with angle closure (63-65). This may be due to the aberrant permeability at the level of iris vascular endothelium or iris pigment epithelium due to alterations in the structural integrity of cellular junctions as result of reduced PLEKHA7. Lower PLEKHA7 expression would also suggest potential abnormalities within the trabecular meshwork cytoarchitecture. Such an alteration may result in aqueous humor outflow restriction, a raised IOP and a predisposition to glaucoma. Based on our HTM actin cytoskeletal experiments showing actin cytoskeletal disorganization, and the compromised cell-cell adhesion in our studies in cells with suppressed PLEKHA7, it suggests similar functional alterations may occur at the cellular level of the endothelial cells within the trabecular meshwork of PACG patients that could affect its contractility and cytoskeleton structure leading to reduced aqueous outflow and an increased intraocular pressure in PACG. (66) Indeed, deformation of trabecular meshwork tissue is often observed in the glaucomatous eye (67, 68), with widened intercellular spaces of trabecular meshwork cells in acute PACG (69). Moreover, the altered PLEKHA7 expression in lens capsule epithelial cells may also have implication in a larger than normal size lens seen often in PACG eyes (70-72). Therefore lowered PLEKHA7 levels may have several consequences at multiple

sites in a PACG eye and further in vivo functional studies and animal studies would be necessary to validate the findings and hypotheses put forth in this study.

In conclusion, we describe a novel function for PLEKHA7 as a Rac1/Cdc42 GAP that regulates cell migration, adhesion and paracellular barrier function. PLEKHA7 and Rac1/Cdc42 colocalize in principal components of the BAB and aqueous humor outflow pathway. The lower PLEKHA7 expression found in PACG patients is a possible common denominator of PACG disease progression as reduced PLEKHA7 will compromise tissue integrity and the BAB, both critical for tissue homeostasis and IOP regulation in the eye.

Materials and Methods

Subjects and Specimens. Subjects were recruited from outpatient clinics of the Singapore National Eye Center (SNEC). The study adhered to the ethical standards in the Declaration of Helsinki and was approved by the institutional review board of the Singapore Eye Research Institute (SERI). After obtaining written informed consent from all subjects, lens capsules were obtained from

53 control, 39 PACG and 64 POAG Chinese subjects during phacoemulsification. Peripheral iris tissue specimens were obtained from 20 PACG and 20 POAG Chinese subjects during trabeculectomy or combined phacoemulsification-trabeculectomy. The specimens were kept in RNA later solution at 4°C for overnight and stored at -80°C on the following day until analysis.

Cell culture (spheroids, HTMC, h-iNPCE) maintenance. h-iNPCE cells were were a kind gift from Prof. M. Coca-Prados (Yale School of Medicine) maintained in DMEM supplemented with 10% fetal bovine serum.Primary HTM purchased and maintained in Fibroblast Medium (Sciencell Research Laboratories) according to manufacturer instructions. Both cell lines were incubated at 37^{o}C with 5% CO_2.

Quantitative real-time PCR. Total RNA was isolated from the lens capsule and whole peripheral iris tissue specimens using the Trizol reagent. Genomic DNA was removed by digestion with DNase I. The resultant RNA sample was measured by Nanodrop 2000 to determine quality and yield before

converting RNA to cDNAwith SuperScript III™ first-strand synthesis system for RT-PCR. Real time qPCR reaction was performed with QuantStudio™ 6 Flex real time qPCR system using SYBR green I chemistry (KAPA Biosystems). Following primers for PLEKHA7 (F-ACAGCCGAGAAGAAGCGGTC ; R- GCCCGCTGTGGAGCTGTTATAGATG) were applied. Relative mRNA expression of *PLEKHA7* in each samples was calculated using the geometric mean of multiple housekeeping genes (73). Thus a normalization factor was calculated for each sample, based on the geometric mean of three housekeeping genes (*GAPDH, B2M* and *HMBS*) found to be the most stable in lens capsule cells, using the geNorm™ VBA applet for Microsoft Excel version 3.5 according to the manufacturer's protocol. Each cDNA sample was analysed in triplicate and average Ct value was taken for relative quantification as described before (74).

Genotyping. Intronic SNP rs11024102 of the *PLEKHA7* gene was genotyped through direct sequencing of the PCR product that was amplified from patient genomic DNA using primers (F: AGGTCGGGGAGGCTTTTGGTTG; R- TTGTACCAGGAAGGGAGGCAGG).

Antibodies. PLEKHA7 antibodies was synthesized by Genemed specifically for our laboratory (Genemed Synthesis), occludin (#sc-133256, Santa Cruz Biotechnology), β-catenin (#26985, Cell Signaling Technology), Rhodamine-phalloidin for Actin (#R415, Invitrogen), Gapdh (#sc-25778, Santa Cruz Biotechnology), Cdc42-GTP (#26905, NewEast Biosciences), Rac1-GTP (#26903, NewEast Biosciences), RhoA-GTP (#26904, NewEast Biosciences), Myc (#sc-40, Santa Cruz Biotechnology), RhoA (#ab54835, Abcam), Rac 1 (#05-389, Millipore), Cdc42 (#sc-87, Santa Cruz Biotechnology), GST-HRP (#MA4004HRP, Thermo Fisher Scientific), and His-HRP (#MA121315HRP, Thermo Fisher Scientific). Aside from HRP pre-conjugated type of primary antibodies, non-conjugated primary antibodies were further incubated with FITC or CY3 labelled Jackson Laboratories secondary antibodies. *Immunoprecipitation.* Cells were lysed with RIPA lysis buffer (50 mM Tris, pH 7.4, 150 mM NaCl, 1% Triton X-100, 1% Sodium deoxycholate, 0.5% Sodium dodecyl sulphate (SDS)) lysis buffer containing 1M HEPES pH7.6, 5M NaCl, 10%NP40, 0.5M EDTA pH8,0.25M PMSF). 500µg of total protein was used for per immunoprecipitation reaction with protein A agarose (Roche).

Western Blotting. Whole-cell extracts containing equal quantities of proteins determined by the Bradford method; or immunoprecipitated proteins were electrophoresed and transferred to nitrocellulose membranes (Biorad). Membranes were blocked with 5% skimmed milk in 0.1% Tween 20 in PBS and incubated with appropriate primary and HRP-conjugated secondary antibodies in 1% skimmed milk in 0.1% Tween 20 in PBS. Membranes were visualized by chemiluminescence using luminata forte (Millipore).

Impedance-measurements. Protocol modified from (75),cells were seeded into FNC-coated 96-well E-Plates (ACEA Biosciences) to a final volume of 200ul and incubated at CO_2 incubator in xCELLigence RTCA (ACEA Biosciences). Impedance data recorded for each well were extracted and analyzed. Triplicates were then performed for each experimental condition for statistical analysis. Calcium switch assay was performed with EDTA (0.5 mM) to disrupt junctions and followed through with RTCA monitoring recovery of junctional impedence after removal of EDTA.

Wound Healing Assay. Cells were seeded in FNC-coated 35mm cell culture dishes at $1x10^6$. Rescue of cells with transient knock-down was carried out using Effectene Transfection Reagent (Qiagen) to transfect PLEKHA7 over-expressing vectors 24h post-knockdown. p10 pipette tips were used to scratch the cell monolayers and images were taken with Nikon Eclipse TS100 Inverted microscope. *In-vitro* wound healing was evaluated by measuring the area of wound from time-lapse images taken by digital camera and calculated by CellSens image analysis program (Olympus).

Plasmids and shRNA. Two sets of PLEKHA7 constructs comprising of a 3363-bp full-length PLEKHA7 fragment were generated with pCI Mammalian Expression Vector (Promega) and pGEX4T-1 (GE Healthcare Life Sciences). PLEKHA7 (NM_175058) Human cDNA ORF clone (Origene Technologies) was used as a PCR template to generate the fragments that were cloned into the NheI/XbaI (pCI-puro) or BamHI/XhoI (pGEX4T-1) sites of the 2 different vectors. Commercially available shRNAs (Sigma-Aldrich) that targeted PLEKHA7 shRNA MS3 (TRCN0000130827) with target sequence CCGGGACCTTCTCAAGGATCGAAGTCTCGAGACTTCGATCCTTGAGAAGG TCTTTTTTG and PLEKHA7 MS2 shRNA (TRCN0000135847) with target sequence

CGGGCCTTCACTCTCAACTTCTGACTCGAGTCAGAA GTTGAGAGTGAAGGCTTTTTTG was selected for subsequent knock-down procedures.

Densitometry measurements of western blots. Quantification of the western bands with Image Studio software (LI-COR Inc.) to quantitateintensity of respective bands on 3 independent experiments. Data represent the mean ± SEM (n=3).Statistical significance of differences between samples are indicated by *P < 0.05 and **P < 0.01. P value less than 0.05 was considered non-significant.

In vitro protein interaction assay. His-Rac1 and His-Cdc42 (100 ng) eluted from beads with buffer containing 100 mM glutathione, pH 7.5, at 4 °C for 15 min were charged with 1 mM GDP, or 200 μM GTP–γS by incubation for 25 min at 30 °C with protein binding buffer (50 mM sodium chloride, 50 mM pH7.4 Tris, 5 mM magnesium chloride). GST-PLEKHA7 proteins (100ng) that remain bound to the GST beads were then incubated at room temperature for 30 min. Three washes of NETN Buffer (20mM pH7.4 Tris, 0.1mM EDTA, 300mM NaCl, 0.5% NP40) were performed to remove unbound or non-specific protein-protein interaction before analysis on SDS-PAGE.

Immunostaining of tissue. Enucleated human eyes were purchased from Lions Eye Institute for Transplant and Research or Singapore General Hospital. Paraffin sections of 4μm were used for immunohistochemistry withLeica Bond Polymer Refine detection kit DS9800. Slides were heated for 20 min at 60˚C and then loaded onto Leica Bond III autostainer for antigen retrievel using Leica Bond ER2 solution for 20 min at 100˚C, antibody incubation follow suit. Primary (1:100) and secondary (1:300) antibodies were diluted in 10% FBS, 0.1% PBS-Tween; and incubated overnight at 4°C and 1h at RT, respectively. Vectashield with 40,6-diamidino-2-phenylindole (DAPI) was applied to the tissues and coverslipped. Confocal microscopy was performed with a Leica SP8 confocal microscope.

Immunofluorescence of cells. Cells were grown on glass coverslips and fixed in 4% PFA for 1 h at 4°C. Cells were blocked in blocking buffer (5% BSA, 0.05% TX-100, PBS) for 1h at room temperature and incubated overnight in the respective primary antibodies at 4°C. Cells were then washed 3 times for 15 min with PBS and incubated with fluorescently-tagged secondary antibodies

for 1h at room temperature followed with addition of Vectashield Anti-fade Mounting Medium with DAPI before coverslipped for analysis.

SIM and 3D analysis of confocal z-stack images. 3D-SIM images were acquired on a Zeiss ELYRA PS.1 super-resolution system equipped with 405, 488, and 561 lasers (50 mW, 200 mW, 200 mW, and 150 mW, respectively) for excitation. A Zeiss 63x, 1.4 NA Plan-Apochromat oil immersion objective lens was used together with a cooled EMCCD camera (iXon EM+ DU885, Andor). 5 images per section per channel were acquired with z-stacks increments at 0.1µm between z-slices. Structured illumination reconstruction and alignment was completed using the ZEN software (Zeiss). Confocal z-stacks were then exported into Imaris® (Bitplane) spot creation module to show 3D distributions of PLEKHA7 and Rac1-GTP signals at the leading cell edges.

GEF activity assay. Full length recombinant GST-PLEKHA7 bacterially expressed in BL21(DE3) and purified on GST beads (GE Healthcare Life Sciences). The purified proteins were visualised by InstantBlue (Expedeon Inc.). *In-vitro* GEF activity assay was carried out using the RhoGEF Exchange Assay BioChem Kit (Cytoskeleton) according to the manufacturer's instructions. with Tecan M200 plate reader. Average of readings at each time-point were normalized against their initial readings at t=0 before the respective GEF proteins were added to initiate the kinetic reactions.

GAP activity assay. Recombinant GST-PLEKHA7 were bacterially expressed in BL21(DE3) and purified on GST beads (GE Healthcare Life Sciences). Purified proteins were visualised by InstantBlue (Expedeon). In-vitro GAP assay was carried out using RhoGAP Assay BioChem Kit (Cytoskeleton) according to the manufacturer's instructions. *t*-test was carried out on absorbance readings taken at 650nm at the end of the reactions. Readings were corrected against the background readings with buffer blank.

Rac1/Cdc42 Activation Assay. Rac1 and Cdc42 activation assays were performed on with small GTPase activation assay kits (Cytoskeleton) according to manufacturer's instructions. 500ug of total cell lysate was used per assay reactionand analysed by SDS-PAGE and Western blot analysis.

Spheroid permeability assay. h-iNPCE cells with transient over-expression or knock-down of PLEKHA7 were cultured in low attachment 6-well plates (Greiner Bio-One). Spheroids were harvested at 72h time point and incubated in media containing dextran-FITC for 2h in CO_2 incubator. Spheroids were washed in PBS and fixed in 4% PFA for 1 h at room temperature. The spheroids were then incubated with 1ug/mL DAPI for 5 minutes and were subsequently mounted onto slides using a cytocentrifuge (Thermo Fisher Scientific) and FluorSave Reagent (Merck Millipore).

Acknowledgements.

The authors acknowledge the Advanced Bio-imaging Core at the Academia, Singapore Health Services. This research is supported by National Medical Research Council, Singapore under its Cooperative Basic Research Grant (CBRG/0032/2013).

Conflict of Interest statement. None declared.

References

1 Thylefors, B., Negrel, A.D., Pararajasegaram, R. and Dadzie, K.Y. (1995) Global data on blindness. *Bulletin of the World Health Organization*, **73**, 115-121.

2 Quigley, H.A., Congdon, N.G. and Friedman, D.S. (2001) Glaucoma in China (and worldwide): changes in established thinking will decrease preventable blindness. *Br J Ophthalmol*, **85**, 1271-1272.

3 Tham, Y.C., Li, X., Wong, T.Y., Quigley, H.A., Aung, T. and Cheng, C.Y. (2014) Global prevalence of glaucoma and projections of glaucoma burden through 2040: a systematic review and meta-analysis. *Ophthalmology*, **121**, 2081-2090.

4 Khor, C.C., Do, T., Jia, H., Nakano, M., George, R., Abu-Amero, K., Duvesh, R., Chen, L.J., Li, Z., Nongpiur, M.E. *et al.* (2016) Genome-wide association study identifies five new susceptibility loci for primary angle closure glaucoma. *Nat Genet*.

5 Vithana, E.N., Khor, C.C., Qiao, C., Nongpiur, M.E., George, R., Chen, L.J., Do, T., Abu-Amero, K., Huang, C.K., Low, S. *et al.* (2012) Genome-wide association analyses identify three new susceptibility loci for primary angle closure glaucoma. *Nat Genet*, **44**, 1142-1146.

6 Lee, M.C., Chan, A.S., Goh, S.R., Hilmy, M.H., Nongpiur, M.E., Hong, W., Aung, T., Hunziker, W. and Vithana, E.N. (2014) Expression of the primary angle closure glaucoma (PACG) susceptibility gene PLEKHA7 in endothelial and epithelial cell junctions in the eye. *Invest Ophthalmol Vis Sci*, **55**, 3833-3841.

7 Kong, X., Liu, X., Huang, X., Mao, Z., Zhong, Y. and Chi, W. (2010) Damage to the blood-aqueous barrier in eyes with primary angle closure glaucoma. *Mol Vis*, **16**, 2026-2032.

8 Tan, J.C., Kalapesi, F.B. and Coroneo, M.T. (2006) Mechanosensitivity and the eye: cells coping with the pressure. *Br J Ophthalmol*, **90**, 383-388.

9 Tam, L.C., Reina-Torres, E., Sherwood, J.M., Cassidy, P.S., Crosbie, D.E., Lutjen-Drecoll, E., Flugel-Koch, C., Perkumas, K., Humphries, M.M., Kiang, A.S. *et al.* (2017) Enhancement of Outflow Facility in the Murine Eye by Targeting Selected Tight-Junctions of Schlemm's Canal Endothelia. *Scientific reports*, **7**, 40717.

10 Freddo, T.F. (2013) A contemporary concept of the blood-aqueous barrier. *Progress in retinal and eye research*, **32**, 181-195.

11 Goel, M., Picciani, R.G., Lee, R.K. and Bhattacharya, S.K. (2010) Aqueous humor dynamics: a review. *The open ophthalmology journal*, **4**, 52-59.

12 Eakins, K.E. (1977) Prostaglandin and non-prostaglandin mediated breeakdown of the blood-aqueous barrier. *Exp Eye Res*, **25 Suppl**, 483-498.

13 Chua, J., Vania, M., Cheung, C.M., Ang, M., Chee, S.P., Yang, H., Li, J. and Wong, T.T. (2012) Expression profile of inflammatory cytokines in aqueous from glaucomatous eyes. *Mol Vis*, **18**, 431-438.

14 Meng, W., Mushika, Y., Ichii, T. and Takeichi, M. (2008) Anchorage of microtubule minus ends to adherens junctions regulates epithelial cell-cell contacts. *Cell*, **135**, 948-959.

15 Pulimeno, P., Bauer, C., Stutz, J. and Citi, S. (2010) PLEKHA7 is an adherens junction protein with a tissue distribution and subcellular localization distinct from ZO-1 and E-cadherin. *PloS one*, **5**, e12207.

16 Pulimeno, P., Paschoud, S. and Citi, S. (2011) A role for ZO-1 and PLEKHA7 in recruiting paracingulin to tight and adherens junctions of epithelial cells. *The Journal of biological chemistry*, **286**, 16743-16750.

17 Guerrera, D., Shah, J., Vasileva, E., Sluysmans, S., Mean, I., Jond, L., Poser, I., Mann, M., Hyman, A.A. and Citi, S. (2016) PLEKHA7 recruits PDZD11 to adherens junctions to stabilize nectins. *The Journal of biological chemistry*.

18 Fanning, A.S., Jameson, B.J., Jesaitis, L.A. and Anderson, J.M. (1998) The tight junction protein ZO-1 establishes a link between the transmembrane protein occludin and the actin cytoskeleton. *The Journal of biological chemistry*, **273**, 29745-29753.

19 Van Itallie, C.M., Fanning, A.S., Bridges, A. and Anderson, J.M. (2009) ZO-1 stabilizes the tight junction solute barrier through coupling to the perijunctional cytoskeleton. *Molecular biology of the cell*, **20**, 3930-3940.

20 Jaalouk, D.E. and Lammerding, J. (2009) Mechanotransduction gone awry. *Nat Rev Mol Cell Biol*, **10**, 63-73.

21 Kouklis, P., Konstantoulaki, M., Vogel, S., Broman, M. and Malik, A.B. (2004) Cdc42 regulates the restoration of endothelial barrier function. *Circulation research*, **94**, 159-166.

22 Wojciak-Stothard, B., Potempa, S., Eichholtz, T. and Ridley, A.J. (2001) Rho and Rac but not Cdc42 regulate endothelial cell permeability. *Journal of cell science*, **114**, 1343-1355.

23 Cascone, I., Giraudo, E., Caccavari, F., Napione, L., Bertotti, E., Collard, J.G., Serini, G. and Bussolino, F. (2003) Temporal and spatial modulation of Rho GTPases during in vitro formation of capillary vascular network. Adherens junctions and myosin light chain as targets of Rac1 and RhoA. *The Journal of biological chemistry*, **278**, 50702-50713.

24 Humphrey, J.D., Dufresne, E.R. and Schwartz, M.A. (2014) Mechanotransduction and extracellular matrix homeostasis. *Nat Rev Mol Cell Biol*, **15**, 802-812.

25 Nusrat, A., Giry, M., Turner, J.R., Colgan, S.P., Parkos, C.A., Carnes, D., Lemichez, E., Boquet, P. and Madara, J.L. (1995) Rho protein regulates tight junctions and perijunctional actin organization in polarized epithelia. *Proc Natl Acad Sci U S A*, **92**, 10629-10633.

26 Hopkins, A.M., Walsh, S.V., Verkade, P., Boquet, P. and Nusrat, A. (2003) Constitutive activation of Rho proteins by CNF-1 influences tight junction structure and epithelial barrier function. *Journal of cell science*, **116**, 725-742.

27 Guillemot, L., Paschoud, S., Jond, L., Foglia, A. and Citi, S. (2008) Paracingulin regulates the activity of Rac1 and RhoA GTPases by recruiting Tiam1 and GEF-H1 to epithelial junctions. *Molecular biology of the cell*, **19**, 4442-4453.

28 Ward, L.D. and Kellis, M. (2012) HaploReg: a resource for exploring chromatin states, conservation, and regulatory motif alterations within sets of genetically linked variants. *Nucleic acids research*, **40**, D930-934.

29 (2015) Human genomics. The Genotype-Tissue Expression (GTEx) pilot analysis: multitissue gene regulation in humans. *Science*, **348**, 648-660.

30 Leslie, R., O'Donnell, C.J. and Johnson, A.D. (2014) GRASP: analysis of genotype-phenotype results from 1390 genome-wide association studies and corresponding open access database. *Bioinformatics*, **30**, i185-194.

31 Nalbant, P., Hodgson, L., Kraynov, V., Toutchkine, A. and Hahn, K.M. (2004) Activation of endogenous Cdc42 visualized in living cells. *Science*, **305**, 1615-1619.

32 Pertz, O. (2010) Spatio-temporal Rho GTPase signaling - where are we now? *Journal of cell science*, **123**, 1841-1850.

33 Ridley, A.J. (2001) Rho GTPases and cell migration. *Journal of cell science*, **114**, 2713-2722.

34 Hehnly, H., Xu, W., Chen, J.L. and Stamnes, M. (2010) Cdc42 regulates microtubule-dependent Golgi positioning. *Traffic*, **11**, 1067-1078.

35 Sander, E.E., van Delft, S., ten Klooster, J.P., Reid, T., van der Kammen, R.A., Michiels, F. and Collard, J.G. (1998) Matrix-dependent Tiam1/Rac signaling in epithelial cells promotes either cell-cell adhesion or cell migration and is regulated by phosphatidylinositol 3-kinase. *The Journal of cell biology*, **143**, 1385-1398.

36 Kardash, E., Reichman-Fried, M., Maitre, J.L., Boldajipour, B., Papusheva, E., Messerschmidt, E.M., Heisenberg, C.P. and Raz, E. (2010) A role for Rho GTPases and cell-cell adhesion in single-cell motility in vivo. *Nature cell biology*, **12**, 47-53; sup pp 41-11.

37 Fukata, M., Nakagawa, M. and Kaibuchi, K. (2003) Roles of Rho-family GTPases in cell polarisation and directional migration. *Curr Opin Cell Biol*, **15**, 590-597.

38 Gustafsson, M.G., Shao, L., Carlton, P.M., Wang, C.J., Golubovskaya, I.N., Cande, W.Z., Agard, D.A. and Sedat, J.W. (2008) Three-dimensional resolution doubling in wide-field fluorescence microscopy by structured illumination. *Biophysical journal*, **94**, 4957-4970.

39 Broman, M.T., Mehta, D. and Malik, A.B. (2007) Cdc42 regulates the restoration of endothelial adherens junctions and permeability. *Trends Cardiovasc Med*, **17**, 151-156.

40 Bruewer, M., Hopkins, A.M., Hobert, M.E., Nusrat, A. and Madara, J.L. (2004) RhoA, Rac1, and Cdc42 exert distinct effects on epithelial barrier via selective structural and biochemical modulation of junctional proteins and F-actin. *Am J Physiol Cell Physiol*, **287**, C327-335.

41 Wallace, S.W., Durgan, J., Jin, D. and Hall, A. (2010) Cdc42 regulates apical junction formation in human bronchial epithelial cells through PAK4 and Par6B. *Molecular biology of the cell*, **21**, 2996-3006.

42 Citi, S., Pulimeno, P. and Paschoud, S. (2012) Cingulin, paracingulin, and PLEKHA7: signaling and cytoskeletal adaptors at the apical junctional complex. *Annals of the New York Academy of Sciences*, **1257**, 125-132.

43 Pampaloni, F., Reynaud, E.G. and Stelzer, E.H. (2007) The third dimension bridges the gap between cell culture and live tissue. *Nat Rev Mol Cell Biol*, **8**, 839-845.

44 Wong, V. and Gumbiner, B.M. (1997) A synthetic peptide corresponding to the extracellular domain of occludin perturbs the tight junction permeability barrier. *The Journal of cell biology*, **136**, 399-409.

45 Wang, W., Dentler, W.L. and Borchardt, R.T. (2001) VEGF increases BMEC monolayer permeability by affecting occludin expression and tight junction assembly. *American journal of physiology. Heart and circulatory physiology*, **280**, H434-440.

46 Tsukita, S., Furuse, M. and Itoh, M. (2001) Multifunctional strands in tight junctions. *Nat Rev Mol Cell Biol*, **2**, 285-293.

47 Guo, M., Breslin, J.W., Wu, M.H., Gottardi, C.J. and Yuan, S.Y. (2008) VE-cadherin and beta-catenin binding dynamics during histamine-induced endothelial hyperpermeability. *Am J Physiol Cell Physiol*, **294**, C977-984.

48 Bazzoni, G. and Dejana, E. (2004) Endothelial cell-to-cell junctions: molecular organization and role in vascular homeostasis. *Physiological reviews*, **84**, 869-901.

49 Dejana, E. (2004) Endothelial cell-cell junctions: happy together. *Nat Rev Mol Cell Biol*, **5**, 261-270.

50 Matter, K. and Balda, M.S. (2003) Functional analysis of tight junctions. *Methods*, **30**, 228-234.

51 Tong, Z., Yang, Z., Patel, S., Chen, H., Gibbs, D., Yang, X., Hau, V.S., Kaminoh, Y., Harmon, J., Pearson, E. *et al.* (2008) Promoter polymorphism of the erythropoietin gene in severe diabetic eye and kidney complications. *Proc Natl Acad Sci U S A*, **105**, 6998-7003.

52 Louis, F., Deroanne, C., Nusgens, B., Vico, L. and Guignandon, A. (2015) RhoGTPases as key players in mammalian cell adaptation to microgravity. *BioMed research international*, **2015**, 747693.

53 Schlegel, N., Meir, M., Spindler, V., Germer, C.T. and Waschke, J. (2011) Differential role of Rho GTPases in intestinal epithelial barrier regulation in vitro. *J Cell Physiol*, **226**, 1196-1203.

54 Gao, Y., Dickerson, J.B., Guo, F., Zheng, J. and Zheng, Y. (2004) Rational design and characterization of a Rac GTPase-specific small molecule inhibitor. *Proc Natl Acad Sci U S A*, **101**, 7618-7623.

55 Erickson, J.W., Zhang, C., Kahn, R.A., Evans, T. and Cerione, R.A. (1996) Mammalian Cdc42 is a brefeldin A-sensitive component of the Golgi apparatus. *The Journal of biological chemistry*, **271**, 26850-26854.

56 Farhan, H. and Hsu, V.W. (2016) Cdc42 and Cellular Polarity: Emerging Roles at the Golgi. *Trends Cell Biol*, **26**, 241-248.

57 Waschke, J., Burger, S., Curry, F.R., Drenckhahn, D. and Adamson, R.H. (2006) Activation of Rac-1 and Cdc42 stabilizes the microvascular endothelial barrier. *Histochem Cell Biol*, **125**, 397-406.

58 Waschke, J., Drenckhahn, D., Adamson, R.H. and Curry, F.E. (2004) Role of adhesion and contraction in Rac 1-regulated endothelial barrier function in vivo and in vitro. *American journal of physiology. Heart and circulatory physiology*, **287**, H704-711.

59 Paul, C. and Robaire, B. (2013) Impaired function of the blood-testis barrier during aging is preceded by a decline in cell adhesion proteins and GTPases. *PloS one*, **8**, e84354.

60 Wang, L., Bittman, R., Garcia, J.G. and Dudek, S.M. (2015) Junctional complex and focal adhesion rearrangement mediates pulmonary endothelial barrier enhancement by FTY720 S-phosphonate. *Microvascular research*, **99**, 102-109.

61 Volcker, H.E. and Naumann, G.O. (1979) Morphology of uveal and retinal edemas in acute and persisting hypotony. *Modern problems in ophthalmology*, **20**, 34-41.

62 Occhiutto, M.L., Freitas, F.R., Maranhao, R.C. and Costa, V.P. (2012) Breakdown of the blood-ocular barrier as a strategy for the systemic use of nanosystems. *Pharmaceutics*, **4**, 252-275.

63 Quigley, H.A., Silver, D.M., Friedman, D.S., He, M., Plyler, R.J., Eberhart, C.G., Jampel, H.D. and Ramulu, P. (2009) Iris cross-sectional area decreases with pupil dilation and its dynamic behavior is a risk factor in angle closure. *J Glaucoma*, **18**, 173-179.

64 Aptel, F. and Denis, P. (2010) Optical coherence tomography quantitative analysis of iris volume changes after pharmacologic mydriasis. *Ophthalmology*, **117**, 3-10.

65 Narayanaswamy, A., Zheng, C., Perera, S.A., Htoon, H.M., Friedman, D.S., Tun, T.A., He, M., Baskaran, M. and Aung, T. (2013) Variations in iris volume with physiologic mydriasis in subtypes of primary angle closure glaucoma. *Invest Ophthalmol Vis Sci*, **54**, 708-713.

66 Petruzzelli, L., Takami, M. and Humes, H.D. (1999) Structure and function of cell adhesion molecules. *The American journal of medicine*, **106**, 467-476.

67 Moses, R.A. (1977) The effect of intraocular pressure on resistance to outflow. *Survey of ophthalmology*, **22**, 88-100.

68 Grierson, I. and Lee, W.R. (1975) The fine structure of the trabecular meshwork at graded levels of intraocular pressure. (1) Pressure effects within the near-physiological range (8-30 mmHg). *Exp Eye Res*, **20**, 505-521.

69 Sihota, R., Goyal, A., Kaur, J., Gupta, V. and Nag, T.C. (2012) Scanning electron microscopy of the trabecular meshwork: understanding the pathogenesis of primary angle closure glaucoma. *Indian J Ophthalmol*, **60**, 183-188.

70 Tomlinson, A. and Leighton, D.A. (1973) Ocular dimensions in the heredity of angle-closure glaucoma. *Br J Ophthalmol*, **57**, 475-486.

71 Lowe, R.F. (1970) Aetiology of the anatomical basis for primary angle-closure glaucoma. Biometrical comparisons between normal eyes and eyes with primary angle-closure glaucoma. *Br J Ophthalmol*, **54**, 161-169.

72 Marchini, G., Pagliarusco, A., Toscano, A., Tosi, R., Brunelli, C. and Bonomi, L. (1998) Ultrasound biomicroscopic and conventional ultrasonographic study of ocular dimensions in primary angle-closure glaucoma. *Ophthalmology*, **105**, 2091-2098.

73 Vandesompele, J., De Preter, K., Pattyn, F., Poppe, B., Van Roy, N., De Paepe, A. and Speleman, F. (2002) Accurate normalization of real-time quantitative RT-PCR data by geometric averaging of multiple internal control genes. *Genome biology*, **3**, RESEARCH0034.

74 Shei, W., Liu, J., Htoon, H.M., Aung, T. and Vithana, E.N. (2013) Differential expression of the Slc4 bicarbonate transporter family in murine corneal endothelium and cell culture. *Mol Vis*, **19**, 1096-1106.

75 Wittchen, E.S., Nishimura, E., McCloskey, M., Wang, H., Quilliam, L.A., Chrzanowska-Wodnicka, M. and Hartnett, M.E. (2013) Rap1 GTPase activation and barrier enhancement in rpe inhibits choroidal neovascularization in vivo. *PloS one*, **8**, e73070.

Legends to Figures

Figure 1. Analysis of *PLEKHA7* mRNA expression level in different patient cohorts. (**A**) Normalized mRNA expression of *PLEKHA7* in lens capsules of PACG, POAG and control subjects as measured by quantitative real-time PCR. Fold changes in *PLEKHA7* gene expression in lens capsules of PACG and POAG compared against non-glaucoma subjects. **(B)** Fold changes in *PLEKHA7* gene expression in peripheral iris tissue of PACG compared against that of POAG subjects (**C**) Genotype-correlated *PLEKHA7* expression in PACG lens capsules. (**D**) Genotype-correlated *PLEKHA7* expression in POAG lens capsules. (**E**) Genotype-correlated *PLEKHA7* expression in normal control lens capsules. Mean fold expression is shown as mean ± SD. *P* value was calculated using a two-tailed t-test comparing either PACG or POAG with control levels or two genotypes. Statistical significance of differences between samples are indicated by $*P < 0.05$ and $**P < 0.01$. *P* value less than 0.05 was considered non-significant (N.S.).

Figure 2. Reduced PLEKHA7 induces loss of cellular architecture. (**A** and **B**) Western blot analysis of HTM whole cell lysates from experimental control nucleofected with pLKO-non-target (pLKO-NT) vector and pLKO-MS3 that harbour PLEKHA7-specific shRNA to render depletion of PLEKHA7. Internal loading control was assessed with Gapdh. (**C** and **D**) Representative time-lapse fluorescence microscopy images of primary HTM cells with or without shRNA-induced PLEKHA7 protein depletion over 72 h. Comparisons of endogenous PLEKHA7 expression level (green) alongside actin (red) were assessed. Nuclei were labelled with DAPI (blue). Scale 20μm. (**E**) The spatial relationship between PLEKHA7 and Actin was analyzed with Pearson's correlation coefficient analysis (all conditions $n > 40$). Data represent the mean ± SEM. Statistical significance of differences between samples are indicated by $*P < 0.05$ and $**P < 0.01$. *P* value less than 0.05 was considered non-significant.

Figure 3. PLEKHA7 is a specific interactor of Rac1 and Cdc42. (**A**) Representative time-lapse fluorescence microscopy images of h-iNPCE cells during cell migration. Endogenous PLEKHA7 (green), Rac1-GTP (red), Cdc42-GTP (red) and RhoA-GTP (red) were labelled and analyzed. Scale

20μm. (**B**) The spatial relationship between PLEKHA7 and respective RhoGTPases were analyzed with Pearson Pearsonearsonth Pearsoent (all conditions $n > 40$). Error bars represent ±SEM. Value of 0 denotes no linear correlation while positive values closer to 1 denote positive correlation of protein pair evaluated. (**C**) PLEKHA7 co-immunoprecipitated with Cdc42 and Rac1 from untransfected h-iNPCE cells. (**D** and **E**) *In vitro* protein binding assays between recombinant proteins. Full-length GST-tagged PLEKHA7 were incubated with either unbound, GTPγS bound or GDP bound His-tagged Cdc42 or Rac1 and analyzed by western blot analysis.

Figure 4. PLEKHA7 is a specific GAP for Rac1 and Cdc42. (**A**) RhoGTPases activation assay showing alteration in endogenous GTP-bound Rac1 and Cdc42 with overexpression or depletion of PLEKHA7 levels. (**B** and **C**) Quantification of immunoprecipitated GTP bound Cdc42 or Rac1 by densitomentry analysis. (**D** and **E**) Enzymatic GAP assays using recombinant GST-tagged PLEKHA7 with either His-tagged Cdc42 or Rac1. p50 RhoGAP domain was included as a positive control. Results are presented as the mean ±SEM from three independent experiments. (**F** and **G**) Kinetic GEF assays measuring kinetics of Cdc42 and Rac1 GTP loading by recombinant GST-tagged PLEKHA7 proteins. Dbl's Big Sister DH/PH GEF domain (hDbs) was included as a positive control. All experimental conditions n=3. Values were statistically tested by t test, error bars represent ± SEM. *P< 0.05 and **$P < 0.01$.

Figure 5. PLEKHA7 modulate wound closure kinetics. (**A**) Migration of h-iNPCE cells was assessed over a period of 8 hours. Control cells representative of endogenous PLEKHA7 protein level were transfected with pCI-puro-Myc or pLKO-NT empty vectors. PLEKHA7 overexpression in h-iNPCE cells was achieved with transfection of pCI-puro PLEKHA7-Myc (PLEKHA7-Myc), while PLEKHA7 silencing was achieved using commercially available PLEKHA7-specific shRNA (pLKO-MS3). Subsequent rescue of PLEKHA7 silenced cells (pLKO-MS3+PLEKHA7-Myc) were analyzed for wound healing efficiency. (**B**) Kinetics of wound healing was expressed as the percentage of the wound closure. n = 4 per group; Values were statistically tested by t test, error bars represent SEM. *P< 0.05 and **P <0.01. (**C**) Confocal microscopy of h-iNPCE, colocalization of endogenous PLEKHA7 (green) and Rac1-GTP (red) were evaluated for fluorescence colocalization based on

relative fluorescence intensity peaks resolved along the yellow line. Scale 20μm. (**D**) 3D-SIM of an actively migrating h-iNPCE cell immunostained with antibodies against PLEKHA7 (green), Rac1-GTP (red) and nucleus (blue). Enrichment of punctate Rac-1 positive focal adhesion complexes were observed at the lamellipodia at the leading edge of the cell. Scale 5μm.

Figure 6. PLEKHA7 is essential for the stabilization of AJC proteins essential for maintenance of blood aqueous barrier function.

(**A**) Recruitment of TJ protein, occludin (red) with different PLEKHA7 (green) protein expression levels in h-iNPCE multicellular 3D spheroids. PLEKHA7/occludin coimmunofluorescence were observed to be stronger with PLEKHA7 overexpression in contrast to control (ctrl) with endogenous level of PLEKHA7 and PLEKHA7-depleted (KD) spheroids. Scale 20μm. (**B**) Significantly stronger AJ protein, β-catenin were observed in h-iNPCE overexpressing PLEKHA7 (Oxp). In contrast, weaker PLEKHA7/occludin, and PLEKHA7/β-catenin colocalization were observed in PLEKHA7 depleted spheroids (KD). Scale 20μm. (**C**) Western blot analysis of whole cell lysates from respective PLEKHA7 h-iNPCE spheroids were evaluated for the expression level of PLEKHA7, level of overexpression (Myc), occludin and β-catenin. Gapdh was included as a loading control. (**D**) Penetration of a fluorescein isothiocyanate (FITC) labelled dextran (dextran-FITC) into h-iNPCE spheroids further substantiated the participation of PLEKHA7 in maintenance of h-iNPCE paracellular barrier function. Greater extent of dextran penetration was observed in spheroids where PLEKHA7 had been depleted (KD) in comparison with the control (Ctrl) and PLEKHA7 overexpressing (Oxp) spheroids. Subsequent rescue of PLEKHA7 depleted spheroids (Res) with PLEKHA7 overexpression construct was found to decrease dextran penetration. Scale 20μm. (**E**) When compared against control (Ctrl), overexpression (PL7 Oxp) or depletion (PL7 KD) of PLEKHA7 showed a significant increment or reduction, respectively, of h-iNPCE impedance values. (**F**) Cumulative TEER differences was observed to be significant and relative to PLEKHA7 expression levels. Data represent mean ± SD of TEER (n = 4). *P < 0.05, **P < 0.01. (**G**) Using control (Ctrl) impedance values as a baseline, recovery kinetics of h-iNPCE calcium-dependent barrier function was faster in cells overexpressing PLEKHA7 (PL7 Oxp) and slower in cells where

PLEKHA7 had been depleted (PL7 KD). Data represent mean ± SD of TEER (n = 4). *P < 0.05, **P < 0.01.

Figure 7. Cdc42-GTP and Rac1-GTP colocalize and interact with PLEKHA7 in PACG-related BAB structures. (**A**) Coimmunofluorescence of PLEKHA7 (green) with Cdc42-GTP (red) is highly expressed in non-pigmented ciliary epithelium (NPCE) and ciliary muscle (CM) but at moderate levels in pigmented ciliary epithelium (PCE). Partial colocalization of PLEKHA7 with Cdc42-GTP is observed in trabecular meshwork (TM) next to SchlemmKH canal (SC) with no fluorescence detected for both PLEKHA7 and Cdc-42-GTP in sclera (S). PLEKHA7 and Cdc42-GTP was highly expressed in iris dilator muscle (IDM) and at moderate level in iris stroma (IS), anterior iris border (AIB) and iris pigmented epithelium (IPE). When observed with higher magnification power, PLEKHA7 and Cdc42-GTP colocalized strongly in endothelium of iris capillaries (IC). (**B**) Rac1-GTP (red) coimmunolabelled with PLEKHA7 (green) showed strong immunopositive signals in BAB-related structures such as NPCE, TM, IDM, CM, IC and iris sphincter muscle (ISM).

Figure 8. PLEKHA7 is a GAP that modulates BAB homeostasis. Schematic drawing of PLEKHA7 as a multifaceted molecule interacting with GTP-bound Rac1 and Cdc42. Maintenance of the BAB at cellular level would require multiple levels of pathway orchestration that involves RhoGTPases, FAK pathway transactivation alongside AJC assembly activities involving cytoskeletal structures within the cell.

Supplementary Material, Figure S1. Annotation of *PLEKHA7* locus in ENCODE. The PLEKHA7 rs11024102 locus as annotated by the publicly available ENCODE project database. The index SNP rs11024102 is located within intron 3 of PLEKHA7 (~27kb downstream of the spice donor site of intron 3) near multiple regulatory elements. Intron 1 (114bp) and 2 (78bp) of PLEKHA7 are small introns and therefore not apparent in the schematic displayed here. (**A**) DNAse 1 hypersensitivity sites (denoting possible sites of open chromatin) at the PLEKHA7 locus, centered on sentinel SNP rs11024102 are shown. No DNAse 1 hypersensitivity sites were observed with the retinal epithelial cell line (cell line #75) within this locus. A list of all cell lines tested can be found in this link: https://genome.ucsc.edu/cgibin/hgc?hgsid=598145267_ZfO4x3J9c6OYxdpX5sCme3AqZRAC&g=htcListItemsAssayed&table=wgEncodeRegDnaseClustered. (**B**) ENCODE annotation

showing the chromatin state, transcription start sites, and transcription factor binding sites at the PLEKHA7 rs11024102 locus.

Supplementary Material, Figure S2. Characterization of in-house PLEKHA7 antibody. (**A**) Schematic representation of location of the epitope recognized by the in-house antibody. The pleckstrin homology domain (PH), two WW interaction domains, SbcC ATPase domain (SbcC), and DUF domain (DUF) of PLEKHA7 are shown (not drawn to scale). (**B**) h-iNPCE overexpressing PLEKHA7-Myc with transfection of C-terminally tagged pCI-puro-PLEKHA7-Myc construct (PLEKHA7-Myc) at 0.5µg were double transfected with either non-target control (pLKO-NT) at 5µg or PLEKHA7-specific shRNA (pLKO-MS3) with increasing dosage from 2.5 to 10µg. Amount of PLEKHA7-Myc was later detected on western with anti-Myc antibody and Gapdh was included as a loading control. (**C**) Specificity of in-house PLEKHA7 antibodies were evaluated by coimmunofluorescence of h-iNPCE cells stained with in-house anti-PLEKHA7 (red), and anti-Myc (green), and DAPI (DNA; blue). Scale 10µm.

Supplementary Material Figure S3. Z-stack of spheroids showing differential recruitment of occludin with PLEKHA7. 3D renderings of confocal z-stacks of apical (Ap) and basal (Ba) layer of spheroids cross-sections. Occludin (red) and PLEKHA7 (green) was coimmunolocalize for analysis of cellular junction enrichment of occludin with h-iNPCE correlating to level of PLEKHA7 expression. DAPI (DNA; blue). Scale 10µm. (**A**) Multicellular 3D spheroid with endogenous occludin and PLEKHA7 (**B**) h-iNPCE spheroid composed of cells overexpressing PLEKHA7-Myc with transfection of C-terminally tagged pCI-puro-PLEKHA7-Myc construct (PLEKHA7-Myc). (**C**) h-iNPCE spheroid with depletion of PLEKHA7 with transfection of PLEKHA7-specific shRNA construct pLKO-MS3.

Supplementary Material, Figure S4. Validation of shRNA mediated PLEKHA7 knockdown as a protein essential for maintenance of h-iNPCE cellular barrier. An alternative vector based shRNA pLKO-MS2 with independent target sites that differ from pLKO-MS3 was used for functional

analysis. Similar to pLKO-MS3 effects, pLKO-MS2 depletion of PLEKHA7 (PL7 KD) when compared against control (Ctrl), and overexpression (PL7 Oxp) showed a significant reduction of h-iNPCE impedance values.

Supplementary Material, Table S1. *PLEKHA7* locus HaploReg annotations.

HaploReg annotations for the sentinel *PLEKHA7* rs11024102 SNP marker and SNPs showing pair-wise r2 > 0.8 with it.

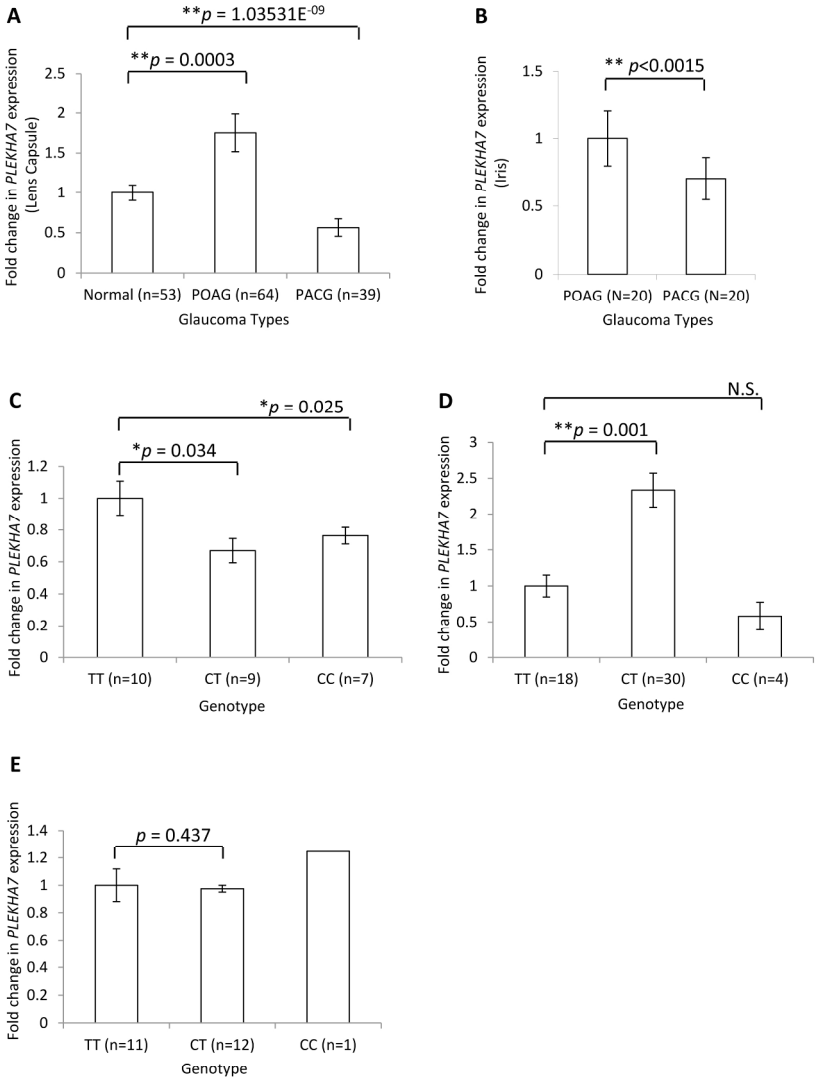

Figure 1

190x254mm (300 x 300 DPI)

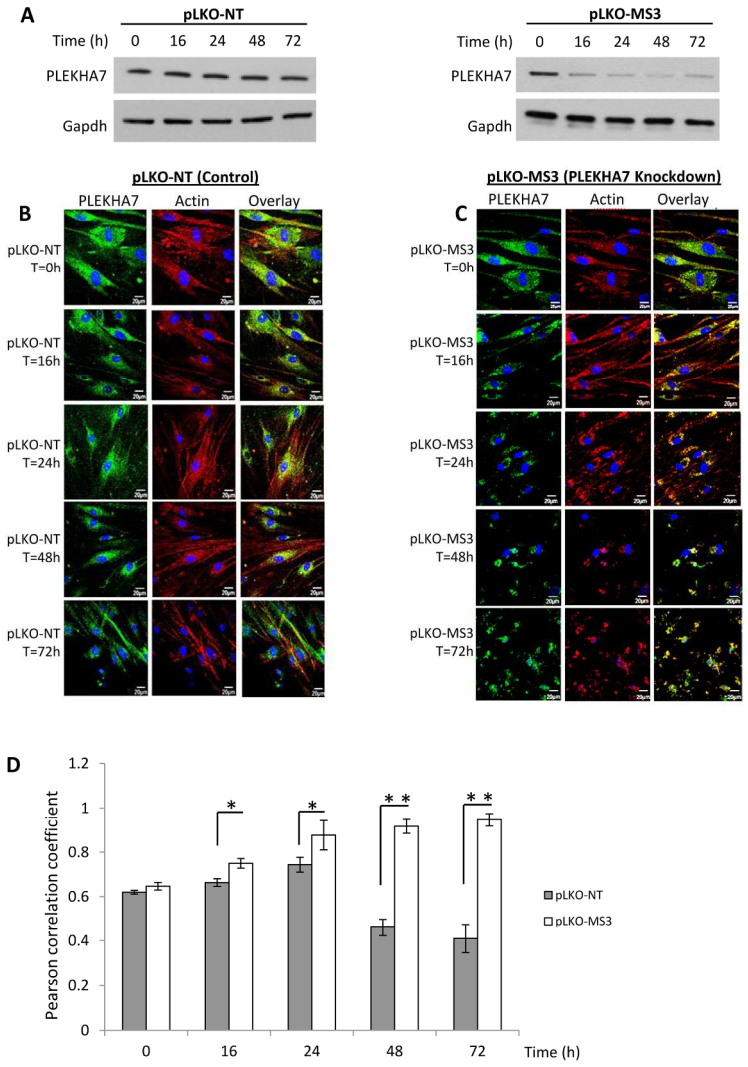

Figure 2

190x254mm (300 x 300 DPI)

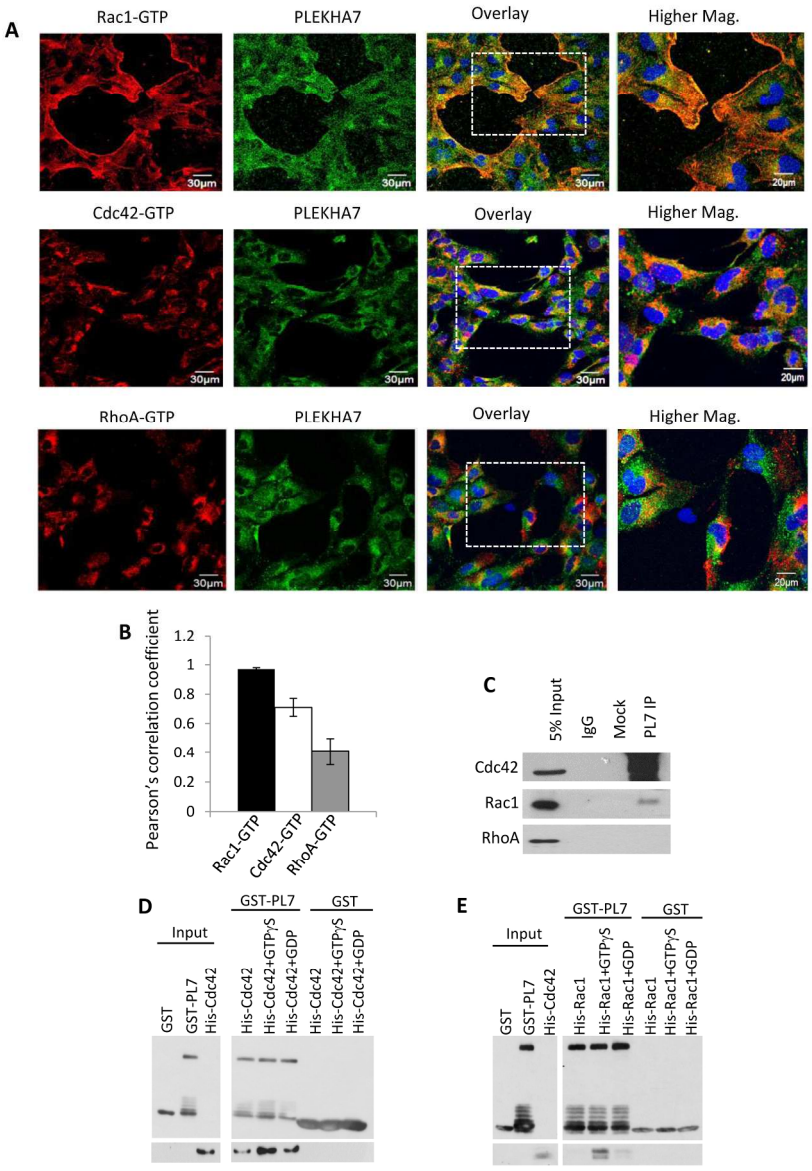

Figure 3

190x254mm (300 x 300 DPI)

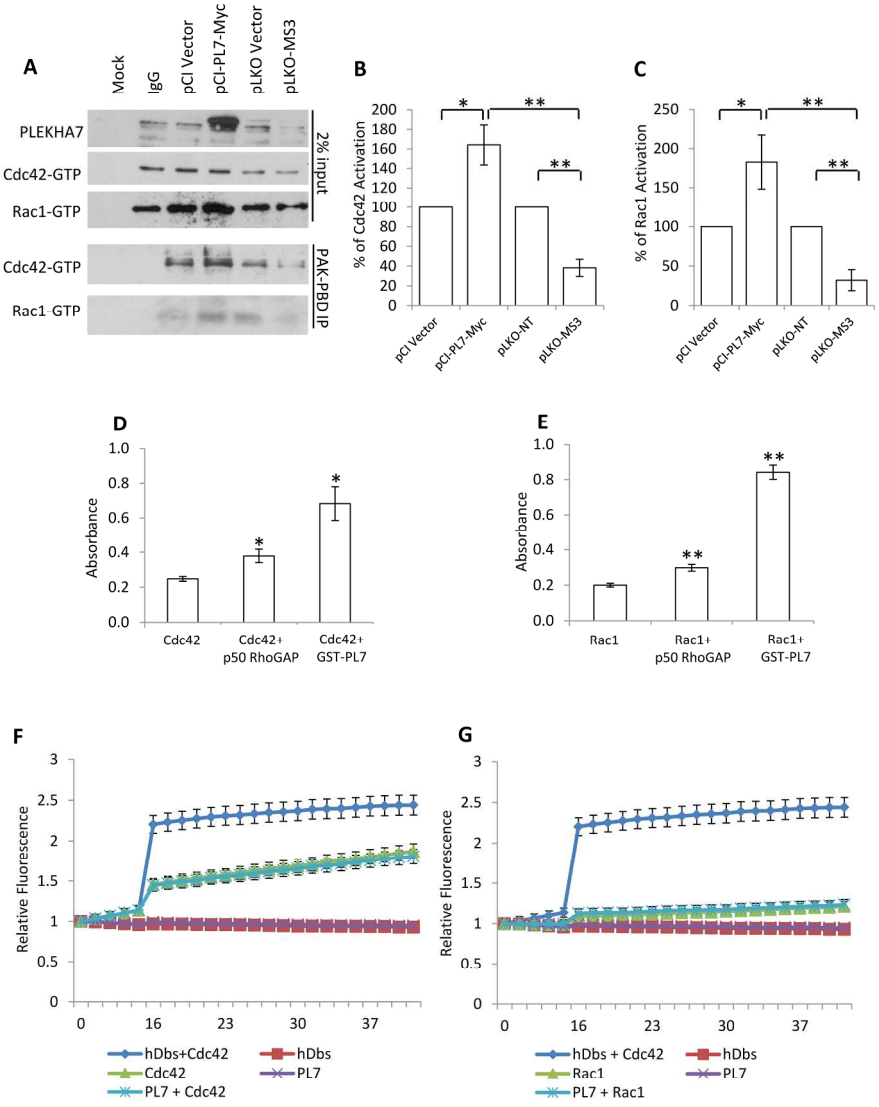

Figure 4

190x254mm (300 x 300 DPI)

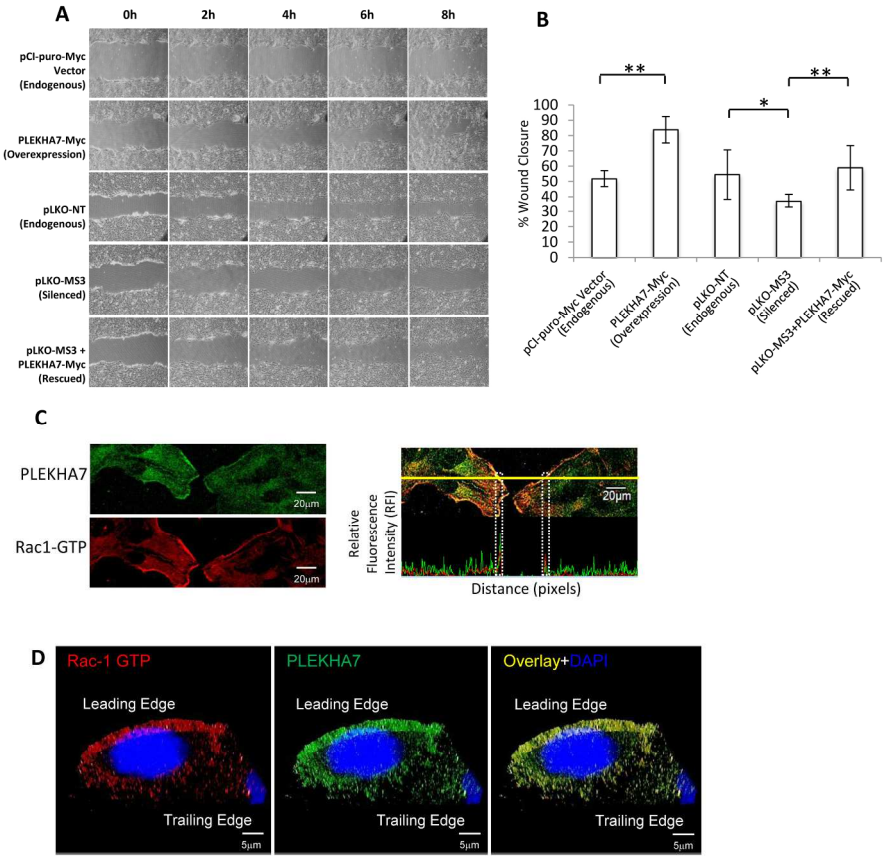

Figure 5

190x254mm (300 x 300 DPI)

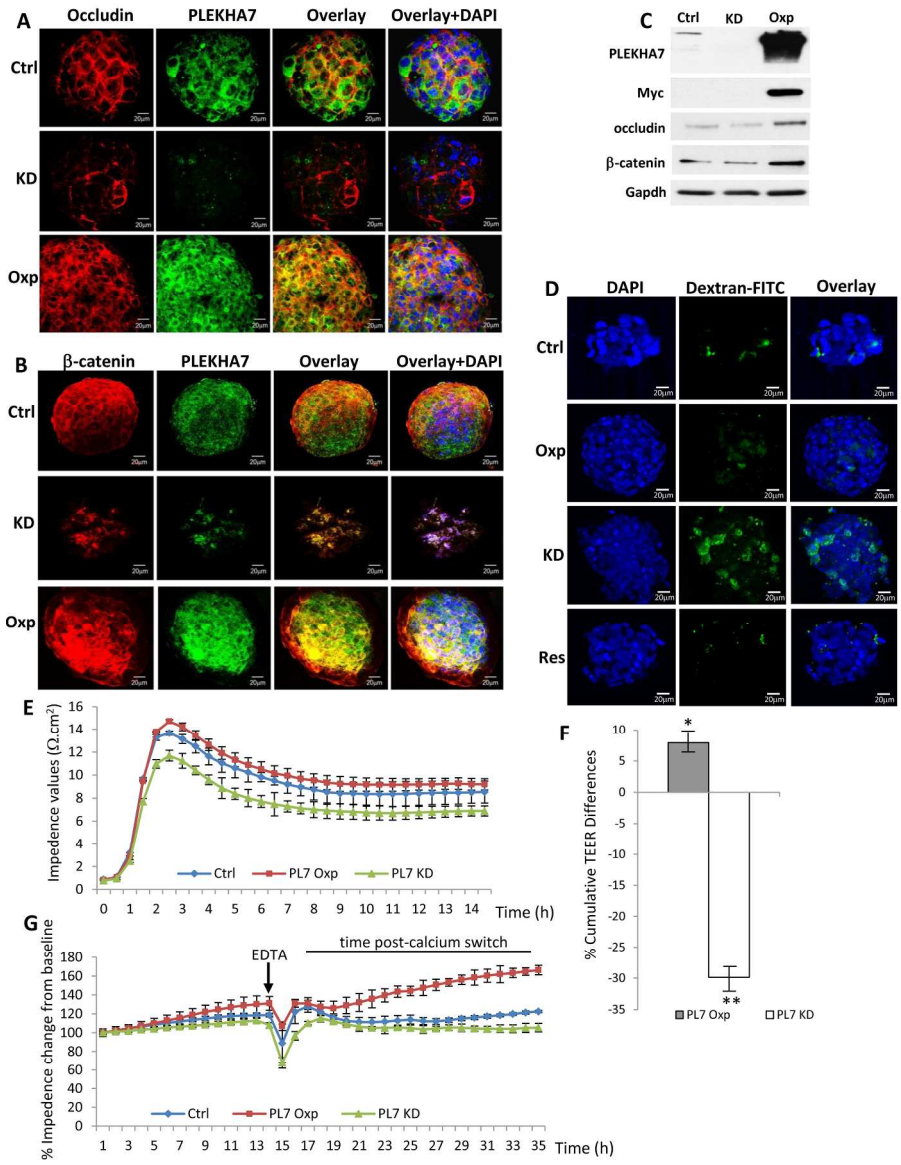

Figure 6

190x254mm (300 x 300 DPI)

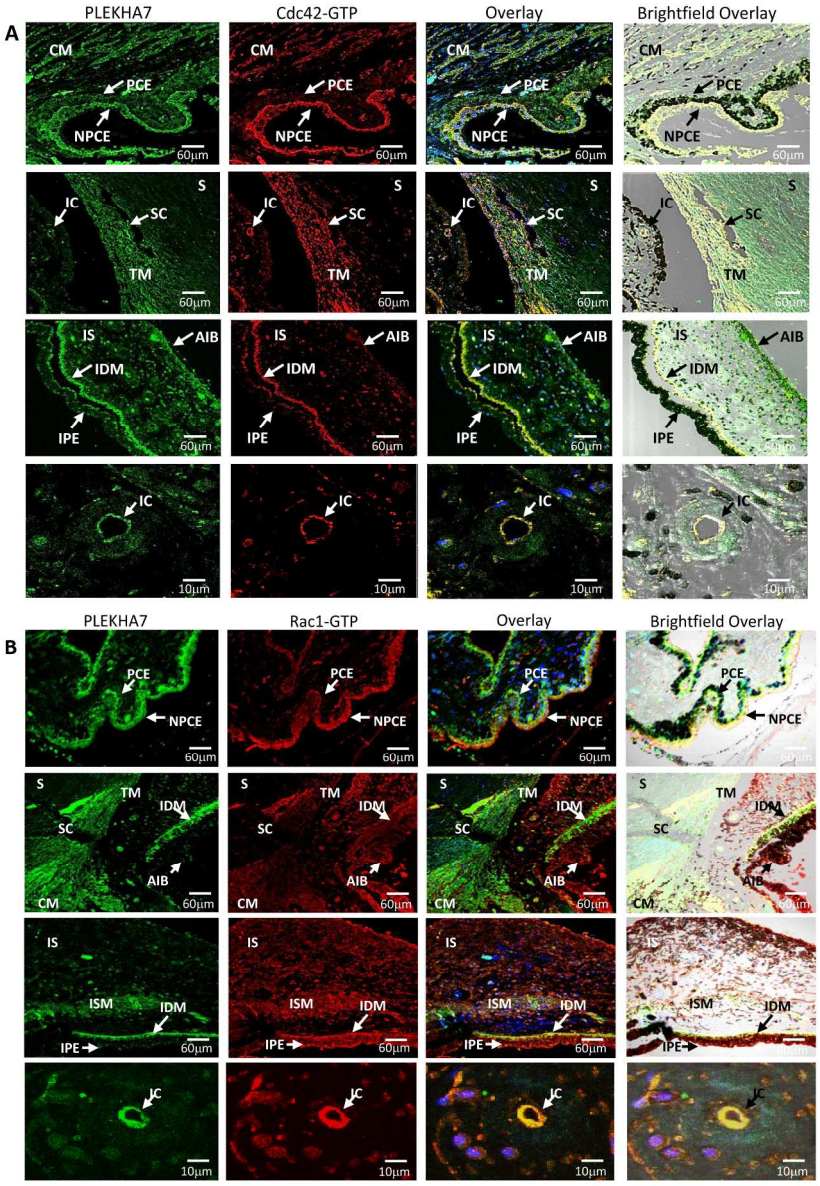

Figure 7

190x254mm (300 x 300 DPI)

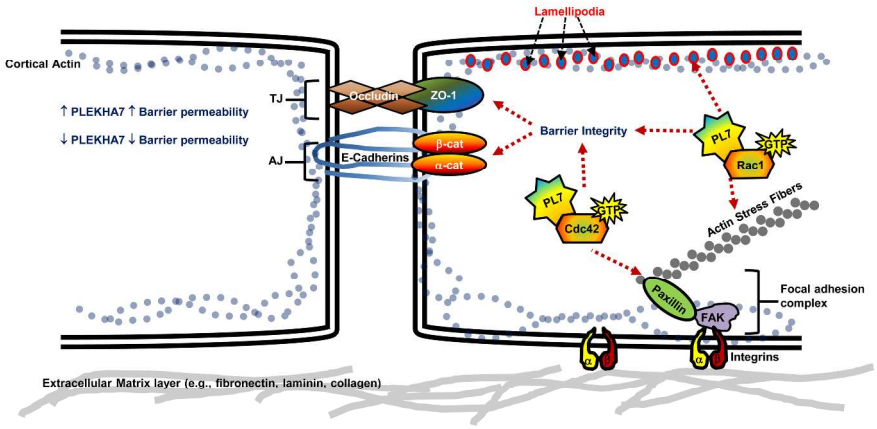

Figure 8

254x338mm (300 x 300 DPI)